Polarizability is a key parameter for molecular electronics

Angélique Gillet, Sébastien Cher, Marine Tassé, Thomas Blon, Sandra Alves, Guillaume Izzet, Bruno Chaudret, Anna Proust, Philippe Demont, Florence Volatron, et al.

Polarizability is a Key Parameter for Molecular Electronics

Angélique Gillet,[a] Sébastien Cher,[a] Marine Tassé,[b] Thomas Blon,[a] Sandra Alves,[c] Guillaume Izzet,[c] Bruno Chaudret,[a] Anna Proust,[c] Phillipe Demont,[d] Florence Volatron,[c,*] and Simon Tricard[a,*]

[a] *Laboratoire de Physique et Chimie des Nano-Objets, INSA, CNRS, Université de Toulouse, Toulouse, France*

[b] *Laboratoire de Chimie de Coordination, CNRS, Université de Toulouse, Toulouse, France*

[c] *Institut Parisien de Chimie Moléculaire, CNRS, Sorbonne Université, Paris, France*

[d] *Institut Carnot – Centre Inter-universitaire de Recherche et d'Ingénierie des Matériaux, INP-ENSIACET, CNRS, Université de Toulouse, Toulouse, France*

[*] *Corresponding authors: florence.volatron@sorbonne-universite.fr, tricard@insa-toulouse.fr*

Supporting information. Experimental section and supplementary characterization data.

Abstract

Identifying descriptors that govern charge transport in molecular electronics is of prime importance for the elaboration of devices. The effects of molecule characteristics, such as size, bulkiness or charge, have been widely reported. Herein, we show that the molecule polarizability can be a crucial parameter to consider. To this end, platinum nanoparticle self-assemblies (PtNP SAs) are synthesized in solution, including a series of polyoxometalates (POMs). The charge of the POM unit can be modified according to the nature of the central heteroatom while keeping its size constant. POM hybrids that display remote terminal thiol functions strongly anchor the PtNP surface to form robust SAs. IV curves, recorded by conductive AFM, show a decrease in Coulomb blockade as the dielectric constant of the POMs increases. In this system, charge transport across molecular junctions can be interpreted as variations in polarizability, which is directly related to the dielectric constant.

One of the main objectives of molecular electronics is to relate the performance of devices to the structure and electronic state of molecules.[1–3] A still open question is what molecular parameters are important to describe the transport of an electron across a molecule.[4,5] The discussion started more than twenty years ago,[6] and first considered resistive organic molecules as tunnel barriers, the shape of which could be tuned by the molecular functional moieties,[7,8] although some examples showed it was not systematical.[9–12] In a first approximation, the current depends exponentially on the length of the molecule, *i.e.* on the width of the tunnel barrier, as stated by Simmons's equation,[13,14] but other considerations state that charge transfer processes should also be taken into account to describe thermally activated transport phenomena.[15] Depending on the system, charge transport across molecules occurs though a competition between tunneling and hopping mechanisms.[16,17] In the last mechanism, the electron gets relaxed and remains temporarily trapped in the accessible orbitals of the molecules, and must be thermally activated to hop on and off. By designing asymmetric molecules where the two mechanisms coexist, it has been possible to fabricate sophisticated molecular electronic components, as *e.g.* rectifiers.[18,19] Here, the nature and accessibility of the orbitals of the molecular junction is a clearly identified parameter that governs the electron transport mechanism, in addition to the molecule size and bulkiness.[20] Some studies also reported that the charge of the molecule can have a significant effect.[21,22] However, very few studies consider the polarizability of the molecule as a key parameter.[23–25] Here, we show that charge effect on electric transport through molecules in nanoparticle self-assemblies can be interpreted as variation of their dielectric constant, which is directly related to their polarizability.

Among the diverse approaches for studying molecular junctions, nanoparticle (NP) self-assemblies (SAs) with functional molecules have been extensively studied, as NPs can be considered as nanoelectrodes that connect molecules.[26–30] In such systems, a large number of molecules are involved and only average behaviors of the composite material is measured. The equivalent circuits are usually referred to as resistors and capacitors in series, the parameters of which vary as a function of the physico-chemical properties of both the molecules and the NPs.[31] Several molecular effects have been reported to influence charge transport in NP SAs, such as *e.g.* the molecule length,[32,33] redox state,[34] conjugation,[35] or spin state.[36] Recently, we demonstrated that using ultra-small NPs

(< 2 nm), it was possible to observe Coulomb blockade at room temperature in NP SAs.[37] This finding was of particular interest since such a blockade was observed at any scale of measurement: nano, micro, or macro. Charge transport was then determined by three parameters: the size of the NPs, the distance between them, and the polarizability of the molecules. However, even if we were able to dissociate effects of such three parameters, it remained very challenging to vary only one at a time. In the present study, we focused on polarizability effects, and thus designed the systems in order to keep the NP size constant (by using the same starting ultra-small PtNP), and the inter-particle distance constant (by choosing series of molecules of the same size). Polarizability was varied by changing the chemical composition of the molecules.

Polyoxometalates (POMs) are polyanionic metal-oxides made of early transition metals (*e.g.* W, Mo) and often contain one or several central heteroatoms (*e.g.* B, P, Al). They have been exploited for uses in molecular electronics, including memories,[38,39] polarizers,[40] rectifiers,[41] or magnetic transistors.[42] Electrical studies have been performed with POMs in diverse forms, as for example thin layers,[43] monolayers,[44] dots on surface,[45] or SAs with quantum dots.[46] There, measurements were performed on assemblies of molecules, but thanks to their robustness, POMs are also suitable for experiments on single molecules,[47] *e.g.* either soldered in a junction[48] or addressed under a STM tip.[49] In the present study, we performed electrical measurements on SAs including PtNPs and POMs. POMs can be functionalized through the covalent anchorage of one or several organic moieties that will interact with the NP surface in order to form stable and robust SAs.[46,50–52] In addition, isostructural POMs displaying different charges can be synthesized by changing the nature of their central heteroatom(s).[53] In the present study, we developed a new series of POM hybrids, based on the Keggin structure, displaying remote thiol functions, where the central atom was varied from Al, to Si and P. The modification of the heteroatom tunes some of their physico-chemical properties such as their charge, and so their polarizability as they all have the same size.

Three POM hybrids of increasing charges, $(TBA)_3[PW_{11}O_{39}\{O(SiC_3H_6SH)_2\}]$, $(TBA)_4[SiW_{11}O_{39}\{O(SiC_3H_6SH)_2\}]$ and $(TBA)_5[AlW_{11}O_{39}\{O(SiC_3H_6SH)_2\}]$, named **POM-P**, **POM-Si** and **POM-Al**, were synthesized by condensation of the organosilane $(OCH_3)_3SiC_3H_6SH$ on the corresponding monolacunar POMs $[XW_{11}O_{39}]^{n-}$ in acidic medium (Fig. 1a – TBA stands for

tetrabutylammonium $(n\text{-}Bu)_4N^+$). The three resulting POM hybrids were prepared as TBA salts to facilitate their dissolution in acetonitrile, in which the PtNPs were also soluble. They were characterized by NMR spectroscopy (Fig. S1 to S4), IR spectroscopy (Fig. S5), mass spectrometry (Fig. S6 to S8), elemental analysis and cyclic voltammetry (CV – Fig. 1b). Detailed interpretation of the POM characterizations is given in supporting information and confirmed their purity and their increasing charges: 3- for **POM-P**, 4- for **POM-Si** and 5- for **POM-Al**. In particular, the reversible and monoelectronic waves observed in CV attested for the absence of protonation. Moreover, the first reduction potential varied with the POMs charge: the less charged **POM-P** (E_{red} = -0.43 V *vs* SCE) was easier to reduce than **POM-Si** (E_{red} = -0.87 V *vs* SCE) than **POM-Al** (E_{red} = -1.26 V *vs* SCE). To support the study, a fourth POM hybrid called **POM-AlH**, which consisted in a protonated form of **POM-Al**, was also isolated. Its formula $(TBA)_{4.1}H_{0.9}[AlW_{11}O_{39}\{O(SiC_3H_6SH)_2\}]$ was assessed by combination of ^1H NMR (Fig. S9) and elemental analysis. The CV of **POM-AlH** displayed multiple waves, confirming its protonated state (Fig. S10).

The PtNPs were synthesized by decomposition of $Pt_2(dba)_3$ (dba = dibenzylideneacetone) under a carbon monoxide (CO) atmosphere in THF, followed by washing of the organic dba ligands with pentane, as previously reported.[37,54] The obtained NPs were dissolved in acetonitrile, to have all the building blocks in a same solvent for SA. Transmission electron microscopy (TEM) pictures showed well-dispersed pristine NPs, with diameters of 1.7 nm ± 0.3 nm (Fig. 1c). Such NPs are particularly interesting since, in addition to their ultra-small sizes, they are "naked", *i.e.* free of organic ligand, as they are only stabilized by CO from the synthesis and acetonitrile, a coordinating solvent. Solutions of PtNPs and of **POM-Al**, **POM-Si**, **POM-P** and **POM-AlH** were mixed together and agitated for two hours to lead to the **SA-Al**, **SA-Si**, **SA-P**, and **SA-AlH** SAs. The ratio between the quantity of POM and the quantity of platinum atoms was chosen equal to 0.2, as it was previously demonstrated to be the equivalence ratio, when mostly all the ligands are coordinated at the NP surface.[37] TEM images showed that microscopic rod-shaped SAs were formed, without any significant morphologic differences between the four systems (Fig. 2a-d). Each SA was constituted by an aggregation of the PtNPs associated to POMs (Fig. 2e and S11).

As already observed for SA between ultra-small PtNPs and molecular entities, a coordination interaction between the functional groups of the molecules and the NP surface was necessary to form coherent SAs.[36,37,55] Here the presence of the thiol arms allows a strong coordination to the NP surface. Indeed, when we mixed the pristine NPs with unfunctionalized $(TBA)_3[PW_{12}O_{40}]$ polyanions, we did not observed any homogeneous SA, but aggregates of POMs decorated by adsorbed PtNPs (Fig. 2f). Fourrier-transform infra-red (FT-IR) spectroscopy confirmed the interaction between the NPs and the POMs. The spectrum of the pristine NPs showed an intense peak at 2040 cm^{-1} corresponding to the vibration of terminal CO, and two smaller peaks at 1815 and 1883 cm^{-1} corresponding to vibrations of bridging CO (Fig. 3). A shift of the vibration of terminal CO towards lower wavenumbers is a signature of the coordination of additional ligands at the NP surface, which turns to be richer in electron. Higher electronic density at the surface implies stronger back-donation from the NP to the antibonding orbitals of the CO molecule, and thus a weaker vibration.[36,56] We can thus deduce that the shift from 2042 cm^{-1} in the pristine PtNPs to 2031 cm^{-1}, 2034 cm^{-1}, 2036 cm^{-1} in **SA-Al**, **SA-Si**, and **SA-P** is a signature of electronic density donation from the POM hybrids to the NP surface, the higher the POM charge the bigger the effect. Interestingly, we noticed that such a vibration was equal to 2035 cm^{-1} for **SA-AlH**, closer to the one of **SA-Si** than of **SA-Al**, and thus suggesting that the trends in donation of electronic density from the POM hybrid to the NP surface depends on the global charge of the POM or POM/proton adduct more than the nature of the central atom. FT-IR measurements confirmed the absence of interaction for unfunctionalized POM, as the CO terminal vibration was measured at 2041 cm^{-1}, *i.e.* without any significant shift, in the mixture of the pristine NPs with $(TBA)_3[PW_{12}O_{40}]$ polyanions (Fig. S12). The SA procedure was repeated with larger PtNPs of 2.0 ± 0.4 nm. We observed similar structuration in TEM (Fig. S13), and the same trends in FT-IR (Fig. S14). This new SA series with larger NPs is denoted as **SA-Al-2**, **SA-Si-2**, **SA-P-2**, and **SA-AlH-2**.

Charge transport measurements were performed by conductive atomic force microscopy (CAFM), coupled to statistical analyses.[37] The SAs were drop-casted on a gold surface and a large number of *I-V* curves (~ 50) were measured by contacting the CAFM tip at different positions of individual objects. The *I-V* curves were normalized at 2V and averaged to compare the current

characteristics of one sample to another (Fig. 4a-b). The non-linear behavior in *I-V* curves was the signature of the presence of Coulomb blockade at room temperature. Besides, for a given series, the non-linearity of the curve, *i.e.* the Coulomb blockade, decreased when the charge of the POM decreased. For example, the non-linearity of the I-V curve was more pronounced in **SA-Al-2**, than in **SA-Si-2**, than in **SA-P-2**. The characteristics of **SA-AlH-2** was situated close to the one of **SA-Si-2**, confirming the FT-IR observation that the physico-chemical properties of SAs with **POM-AlH** were closer to the ones of **POM-Si** than to the ones of **POM-Al**.

The electron mobility in a NP SA in a Coulomb blockade regime is limited by the charging energy of a NP, defined as $E_C \sim e^2/(2\pi\varepsilon_r\varepsilon_0 d\ ln(s/(s-d))$, where e is the charge of the electron, ε_0 the permittivity of vacuum, ε_r the dielectric constant of the medium surrounding the particles, d the particle diameter, and s the center-to-center distance between two particles.[33,57] The s, d and ε_r parameters can be determined experimentally. The size d of the NPs was measured from size distribution on TEM pictures for each sample, and was equal in average to 1.6 and 2.0 nm for each series of SA (Fig. S11, S13 and Table S1). Small angle X-ray scattering (SAXS) measurements were performed on **SA-Si** and **SA-Si-2** SAs to determine the s values. Broad peaks centered at 0.26 and 0.22 $Å^{-1}$ were observed for the SAs with small and large NP, meaning that NPs were separated from each other by an average correlation distance s equal to 2.4 and 2.9 nm in each series (Fig. S15 and Table S1).[58] We can notice that for each series, the average interparticle distance $s - d$ is about 0.8-0.9 nm, *i.e.* the same order of magnitude as the size of a Keggin-type POM. Finally, the dielectric constant of the POMs was determined by dielectric spectroscopy on powders of free molecules: ε_r = 3.10 for **POM-Al**, 3.36 for **POM-Si**, 3.97 for **POM-P** and 3.51 for **POM-AlH** (Table S1). For the dielectric constant too, the properties of **POM-AlH** were close to the one of **POM-Si**, as observed on the IV curves and the IR spectra. As already demonstrated, even if no specific mechanistic model exist at room temperature for ultra-small NP SAs, current characteristics can phenomenologically be described by the equation $I \propto V^{\xi}$.[37] ξ is a scaling exponent related to current paths through the NP SA, and depends on the SA dimensionality.[57,59] For example, it is generally found between 2 and 3.5 in three dimensional systems.[60] We observed that the fitted ξ increased when the calculated E_C increased (Fig. 4c and Table S1). In the present series, the charging energy E_C increases with the charge and decreases

with the dielectric constant of the molecules. Indeed, charge and dielectric constant are linked to each other: the dielectric constant is the macroscopic parameter that reflects the microscopic polarizability of the molecules. As all the POMs have the same size, increasing the charge number corresponds to decreasing the polarizability.[61]

If we now look at the current for a given voltage on the IV curves, we see that it increases from Al to Si to P, meaning that the charge transport rate increases. Indeed, if we consider a pure POM molecule, the first reduction potential measured by CV increased within this series (the POM is easier to reduce), reflecting a decrease of the LUMO energy, as calculated by DFT.[53] As the Fermi energy of the PtNPs remains constant (since they are the same NPs) and below the POM LUMOs, the energies of theses orbitals are getting closer, which decreases the tunnel barrier of charge transfer across the POM. In addition, more redox peaks in a same CV window may indicate more possible conduction channels for charge transport, and thus higher conductivity. Although coherent with the experimental observations, such considerations on single POMs should be taken into account with caution: CV are measured on well-dispersed molecules in solution and DFT calculation are performed on molecule in "gas phase". But the composite material includes hundreds of PtNPs and POM in series, and POMs are known to be very dependent to external conditions (nature of solvent, of the counter-cation, etc.). A new atomistic modelling framework would thus be needed to fully interpret the results presented here.

In summary, we synthesized a new series of Keggin-type POM hybrids of different charges: **POM-Al** (5-), **POM-Si** (4-), **POM-P** (3-) and **POM-AlH** (~4-). Thanks to their thiol arms, it was possible to elaborate robust and homogeneous SAs with ultra-small PtNPs, on which we succeeded to perform CAFM charge transport measurements. The system was in a Coulomb blockade regime, at room temperature, and the key molecular parameter to describe charge transport was found to be the polarizability of the POM. Such a polarizability is directly linked to the dielectric constant of the molecular system, as described by the Clausius–Mossotti model, which might eventually be adapted to take into account the geometry of the systems at the nanometer scale.[62] Besides, even if trends in charge transport can be considered in terms of LUMO energy levels,[44] one should keep in mind that in an experimental setup, molecules are not standing by themselves and that molecular aspects cannot

be fully decorrelated from the properties of the electrodes, the geometry of the leads and the associated Fermi electronic occupation distribution.[63] The present study is about charge transport in ultra-small NP SA in the Coulomb blockade regime, but polarizability can definitely be considered in other approaches of molecular electronics and its variations can be an important parameter for rationalizing charge transport across molecular junctions.

Acknowledgements

The authors acknowledge Josep M. Poblet for insightful discussion. Financial support from Agence Nationale de la Recherche (PhoCatSA grant ANR-10-LABX-0037-NEXT, and MOSC grant ANR-18-CE09-0007) is acknowledged. This study has been partially supported through the EUR grant NanoX n° ANR-17-EURE-0009 in the framework of the Programme des Investissements d'Avenir.

Conflicts of interest

The authors declare no conflict of interest.

Keywords

Molecular electronics, Polarizability, Platinum nanoparticles, Polyoxometalates, Self-assembly

References

[1] S. J. van der Molen, R. Naaman, E. Scheer, J. B. Neaton, A. Nitzan, D. Natelson, N. J. Tao, H. S. J. van der Zant, H. Mayor, M. Ruben, M. Reed, M. Calame, *Nat. Nanotechnol.* **2013**, *8*, 385–389.
[2] S. Elke, C. J. Carlos, *Molecular Electronics: An Introduction To Theory And Experiment (2nd Edition)*, World Scientific, **2017**.
[3] P. T. Mathew, F. Fang, *Engineering* **2018**, *4*, 760–771.
[4] I. Kanelidis, T. Kraus, *Beilstein J. Nanotechnol.* **2017**, *8*, 2625–2639.
[5] M. Schwarze, C. Gaul, R. Scholz, F. Bussolotti, A. Hofacker, K. S. Schellhammer, B. Nell, B. D. Naab, Z. Bao, D. Spoltore, K. Vandewal, J. Widmer, S. Kera, N. Ueno, F. Ortmann, K. Leo, *Nat. Mater.* **2019**, *18*, 242–248.
[6] A. Nitzan, M. A. Ratner, *Science* **2003**, *300*, 1384–1389.
[7] W. Y. Kim, K. S. Kim, *Acc. Chem. Res.* **2010**, *43*, 111–120.
[8] N. Shivran, S. P. Koiry, C. Majumder, A. K. Chauhan, D. K. Aswal, S. Chattopadhyay, S. Mula, *Phys. Chem. Chem. Phys.* **2020**, *22*, 2098–2104.
[9] M. M. Thuo, W. F. Reus, F. C. Simeone, C. Kim, M. D. Schulz, H. J. Yoon, G. M. Whitesides, *J. Am. Chem. Soc.* **2012**, *134*, 10876–10884.

[10] H. J. Yoon, N. D. Shapiro, K. M. Park, M. M. Thuo, S. Soh, G. M. Whitesides, *Angew. Chem. Int. Ed.* **2012**, *51*, 4658–4661.
[11] H. J. Yoon, C. M. Bowers, M. Baghbanzadeh, G. M. Whitesides, *J. Am. Chem. Soc.* **2014**, *136*, 16–19.
[12] G. D. Kong, M. Kim, H.-J. Jang, K.-C. Liao, H. J. Yoon, *Phys. Chem. Chem. Phys.* **2015**, *17*, 13804–13807.
[13] J. G. Simmons, *J. Appl. Phys.* **1963**, *34*, 238–239.
[14] M. M. Thuo, W. F. Reus, C. A. Nijhuis, J. R. Barber, C. Kim, M. D. Schulz, G. M. Whitesides, *J. Am. Chem. Soc.* **2011**, *133*, 2962–2975.
[15] L. Yuan, L. Wang, A. R. Garrigues, L. Jiang, H. V. Annadata, M. Anguera Antonana, E. Barco, C. A. Nijhuis, *Nat. Nanotechnol.* **2018**, *13*, 322–329.
[16] Q. Lu, K. Liu, H. Zhang, Z. Du, X. Wang, F. Wang, *ACS Nano* **2009**, *3*, 3861–3868.
[17] X. Song, B. Han, X. Yu, W. Hu, *Chem. Phys.* **2020**, *528*, 110514.
[18] H. J. Yoon, K.-C. Liao, M. R. Lockett, S. W. Kwok, M. Baghbanzadeh, G. M. Whitesides, *J. Am. Chem. Soc.* **2014**, *136*, 17155–17162.
[19] G. D. Kong, M. Kim, S. J. Cho, H. J. Yoon, *Angew. Chem. Int. Ed.* **2016**, *55*, 10307–10311.
[20] L. O. Jones, M. A. Mosquera, M. A. Ratner, G. C. Schatz, *J. Phys. Chem. C* **2020**, *124*, 3233–3241.
[21] H. Nakanishi, K. J. M. Bishop, B. Kowalczyk, A. Nitzan, E. A. Weiss, K. V. Tretiakov, M. M. Apodaca, R. Klajn, J. F. Stoddart, B. A. Grzybowski, *Nature* **2009**, *460*, 371–375.
[22] H. Moreira, J. Grisolia, N. M. Sangeetha, N. Decorde, C. Farcau, B. Viallet, K. Chen, G. Viau, L. Ressier, *Nanotechnology* **2013**, *24*, 095701.
[23] S. K. S. Mazinani, R. V. Meidanshahi, J. L. Palma, P. Tarakeshwar, T. Hansen, M. A. Ratner, V. Mujica, *J. Phys. Chem. C* **2016**, *120*, 26054–26060.
[24] M. Baghbanzadeh, L. Belding, L. Yuan, J. Park, M. H. Al-Sayah, C. M. Bowers, G. M. Whitesides, *J. Am. Chem. Soc.* **2019**, *141*, 8969–8980.
[25] X. Chen, H. V. Annadata, B. Kretz, M. Zharnikov, X. Chi, X. Yu, D. A. Egger, C. A. Nijhuis, *J. Phys. Chem. Lett.* **2019**, *10*, 4142–4147.
[26] A. Zabet-Khosousi, A.-A. Dhirani, *Chem. Rev.* **2008**, *108*, 4072–4124.
[27] M. Pauly, J.-F. Dayen, D. Golubev, J.-B. Beaufrand, B. P. Pichon, B. Doudin, S. Bégin-Colin, *Small* **2012**, *8*, 108–115.
[28] Y. Zhou, S.-T. Han, Z.-X. Xu, V. A. L. Roy, *Adv. Mater.* **2012**, *24*, 1247–1251.
[29] A. Nag, D. S. Chung, D. S. Dolzhnikov, N. M. Dimitrijevic, S. Chattopadhyay, T. Shibata, D. V. Talapin, *J. Am. Chem. Soc.* **2012**, *134*, 13604–13615.
[30] J. Liao, S. Blok, S. J. van der Molen, S. Diefenbach, A. W. Holleitner, C. Schönenberger, A. Vladyka, M. Calame, *Chem Soc Rev* **2015**, *44*, 999–1014.
[31] H. Nesser, J. Grisolia, A. Mlayah, T. Alnasser, D. Lagarde, B. Viallet, L. Ressier, *Mater. Today Nano* **2018**, *4*, 38–45.
[32] D. Conklin, S. Nanayakkara, T.-H. Park, M. F. Lagadec, J. T. Stecher, M. J. Therien, D. A. Bonnell, *Nano Lett.* **2012**, *12*, 2414–2419.
[33] J. Dugay, R. P. Tan, M. Ibrahim, C. Garcia, J. Carrey, L.-M. Lacroix, P.-F. Fazzini, G. Viau, M. Respaud, *Phys. Rev. B* **2014**, *89*, 041406.
[34] J. Liao, J. S. Agustsson, S. Wu, C. Schönenberger, M. Calame, Y. Leroux, M. Mayor, O. Jeannin, Y.-F. Ran, S.-X. Liu, S. Decurtins, *Nano Lett.* **2010**, *10*, 759–764.
[35] S. J. van der Molen, J. Liao, T. Kudernac, J. S. Agustsson, L. Bernard, M. Calame, B. J. van Wees, B. L. Feringa, C. Schönenberger, *Nano Lett.* **2009**, *9*, 76–80.
[36] S. Usmani, M. Mikolasek, A. Gillet, J. Sanchez Costa, M. Rigoulet, B. Chaudret, A. Bousseksou, B. Lassalle-Kaiser, P. Demont, G. Molnár, L. Salmon, J. Carrey, S. Tricard, *Nanoscale* **2020**, *12*, 8180–8187.
[37] S. Tricard, O. Said-Aizpuru, D. Bouzouita, S. Usmani, A. Gillet, M. Tassé, R. Poteau, G. Viau, P. Demont, J. Carrey, B. Chaudret, *Mater Horiz* **2017**, *4*, 487–492.
[38] C. Busche, L. Vilà-Nadal, J. Yan, H. N. Miras, D.-L. Long, V. P. Georgiev, A. Asenov, R. H. Pedersen, N. Gadegaard, M. M. Mirza, D. J. Paul, J. M. Poblet, L. Cronin, *Nature* **2014**, *515*, 545–549.

[39] X. Chen, P. Huang, X. Zhu, S. Zhuang, H. Zhu, J. Fu, A. S. Nissimagoudar, W. Li, X. Zhang, L. Zhou, Y. Wang, Z. Lv, Y. Zhou, S.-T. Han, *Nanoscale Horiz.* **2019**, *4*, 697–704.
[40] C. Kato, R. Machida, R. Maruyama, R. Tsunashima, X.-M. Ren, M. Kurmoo, K. Inoue, S. Nishihara, *Angew. Chem. Int. Ed.* **2018**, *57*, 13429–13432.
[41] S. Sherif, G. Rubio-Bollinger, E. Pinilla-Cienfuegos, E. Coronado, J. C. Cuevas, N. Agraït, *Nanotechnology* **2015**, *26*, 291001.
[42] J. de Bruijckere, P. Gehring, M. Palacios-Corella, M. Clemente-León, E. Coronado, J. Paaske, P. Hedegård, H. S. J. van der Zant, *Phys. Rev. Lett.* **2019**, *122*, 197701.
[43] A. Balliou, M. Bouroushian, A. M. Douvas, G. Skoulatakis, S. Kennou, N. Glezos, *Nanotechnology* **2018**, *29*, 275204.
[44] M. Laurans, K. Dalla Francesca, F. Volatron, G. Izzet, D. Guerin, D. Vuillaume, S. Lenfant, A. Proust, *Nanoscale* **2018**, *10*, 17156–17165.
[45] K. Dalla Francesca, S. Lenfant, M. Laurans, F. Volatron, G. Izzet, V. Humblot, C. Methivier, D. Guerin, A. Proust, D. Vuillaume, *Nanoscale* **2019**, *11*, 1863–1878.
[46] B. Martinez, C. Livache, E. Meriggio, X. Z. Xu, H. Cruguel, E. Lacaze, A. Proust, S. Ithurria, M. G. Silly, G. Cabailh, F. Volatron, E. Lhuillier, *J. Phys. Chem. C* **2018**, *122*, 26680–26685.
[47] K. Y. Monakhov, M. Moors, P. Kögerler, in *Adv. Inorg. Chem.*, Elsevier, **2017**, pp. 251–286.
[48] C. Wu, X. Qiao, C. M. Robertson, S. J. Higgins, C. Cai, R. J. Nichols, A. Vezzoli, *Angew. Chem. Int. Ed.* **2020**, DOI 10.1002/anie.202002174.
[49] O. Linnenberg, M. Moors, A. Notario-Estévez, X. López, C. de Graaf, S. Peter, C. Baeumer, R. Waser, K. Yu. Monakhov, *J. Am. Chem. Soc.* **2018**, *140*, 16635–16640.
[50] G. Izzet, F. Volatron, A. Proust, *Chem. Rec.* **2017**, *17*, 250–266.
[51] O. Makrygenni, E. Secret, A. Michel, D. Brouri, V. Dupuis, A. Proust, J.-M. Siaugue, R. Villanneau, *J. Colloid Interface Sci.* **2018**, *514*, 49–58.
[52] C. Martin, K. Kastner, J. M. Cameron, E. Hampson, J. Alves Fernandes, E. K. Gibson, D. A. Walsh, V. Sans, G. N. Newton, *Angew. Chem. Int. Ed.* **2020**, *59*, 14331–14335.
[53] I.-M. Mbomekallé, X. López, J. M. Poblet, F. Sécheresse, B. Keita, L. Nadjo, *Inorg. Chem.* **2010**, *49*, 7001–7006.
[54] S. Gomez, L. Erades, K. Philippot, B. Chaudret, V. Collière, O. Balmes, J.-O. Bovin, *Chem. Commun.* **2001**, 1474–1475.
[55] G. Manai, H. Houimel, M. Rigoulet, A. Gillet, P.-F. Fazzini, A. Ibarra, S. Balor, P. Roblin, J. Esvan, Y. Coppel, B. Chaudret, C. Bonduelle, S. Tricard, *Nat. Commun.* **2020**, *11*, 2051.
[56] C. Dablemont, P. Lang, C. Mangeney, J.-Y. Piquemal, V. Petkov, F. Herbst, G. Viau, *Langmuir* **2008**, *24*, 5832–5841.
[57] C. T. Black, *Science* **2000**, *290*, 1131–1134.
[58] N. Decorde, N. M. Sangeetha, B. Viallet, G. Viau, J. Grisolia, A. Coati, A. Vlad, Y. Garreau, L. Ressier, *Nanoscale* **2014**, *6*, 15107–15116.
[59] A. A. Middleton, N. S. Wingreen, *Phys. Rev. Lett.* **1993**, *71*, 3198.
[60] P. Yang, I. Arfaoui, T. Cren, N. Goubet, M.-P. Pileni, *Nano Lett.* **2012**, *12*, 2051–2055.
[61] T. Buchecker, P. Schmid, S. Renaudineau, O. Diat, A. Proust, A. Pfitzner, P. Bauduin, *Chem. Commun.* **2018**, *54*, 1833–1836.
[62] A. Natan, N. Kuritz, L. Kronik, *Adv. Funct. Mater.* **2010**, *20*, 2077–2084.
[63] A. R. Garrigues, L. Wang, E. del Barco, C. A. Nijhuis, *Nat. Commun.* **2016**, *7*, 11595.

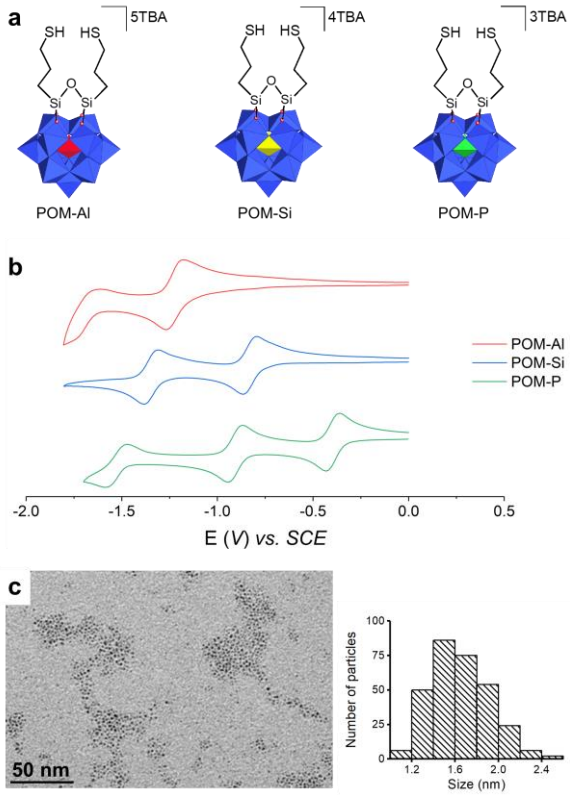

Figure 1. Building blocks. a) Chemical structure of the **POM-Al**, **POM- Si** and **POM-P** polyanions. b) Cyclic voltammograms at a glassy carbon electrode of **POM-Al**, **POM- Si** and **POM-P (0.1V.s^{-1})**. c) TEM picture and size distribution of the pristine ultra-small (1.7 ± 0.3 nm) Pt nanoparticles.

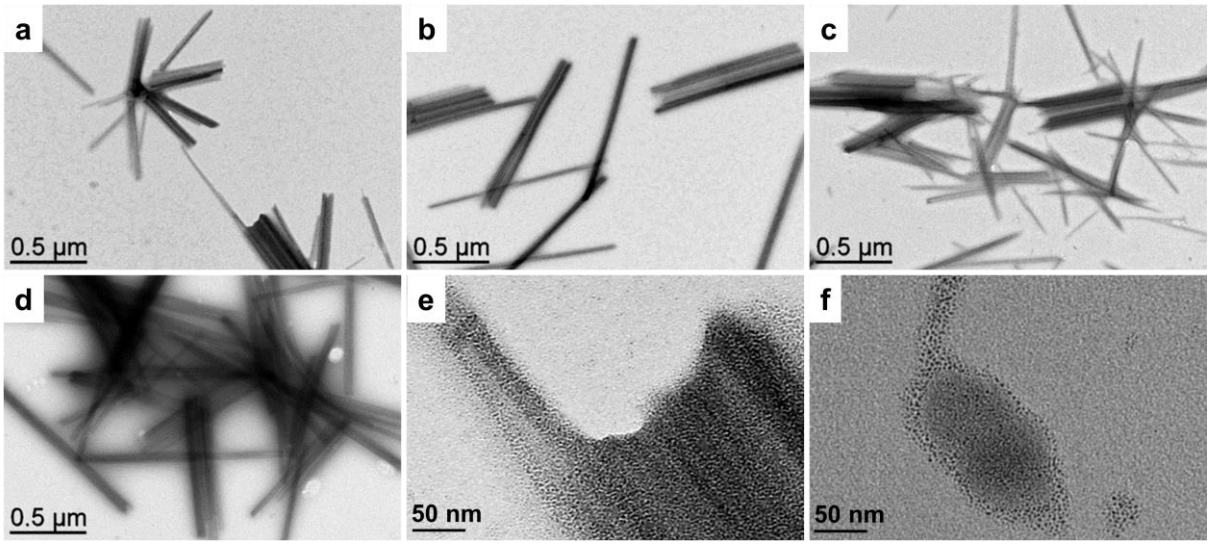

Figure 2. TEM pictures of self-assemblies of Pt nanoparticles and POM: a) **SA-Al**, b) **SA-Si**, c) **SA-P**, d) **SA-AlH**, e) zoom on **SA-P**, and f) TEM picture on mixture of Pt nanoparticles and unfunctionalized $(TBA)_3[PW_{12}O_{40}]$ polyanions.

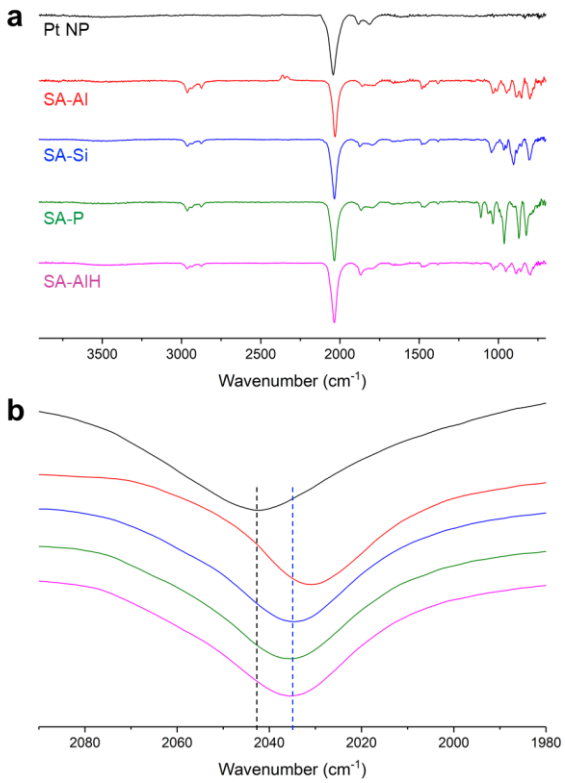

Figure 3. Infrared spectra of the pristine Pt nanoparticles and of the **SA-Al**, **SA-Si**, **SA-P**, and **SA-AlH** self-assemblies: a) full spectra and b) zoom on the terminal CO region (the baselines are shifted for clarity – the dashed lines are a guide for the eye); peak maxima: **PtNP**: 2042 cm^{-1}, **SA-Al**: 2031 cm^{-1}, **SA-Si**: 2034 cm^{-1}, **SA-P**: 2036 cm^{-1}, and **SA-AlH**: 2035 cm^{-1}.

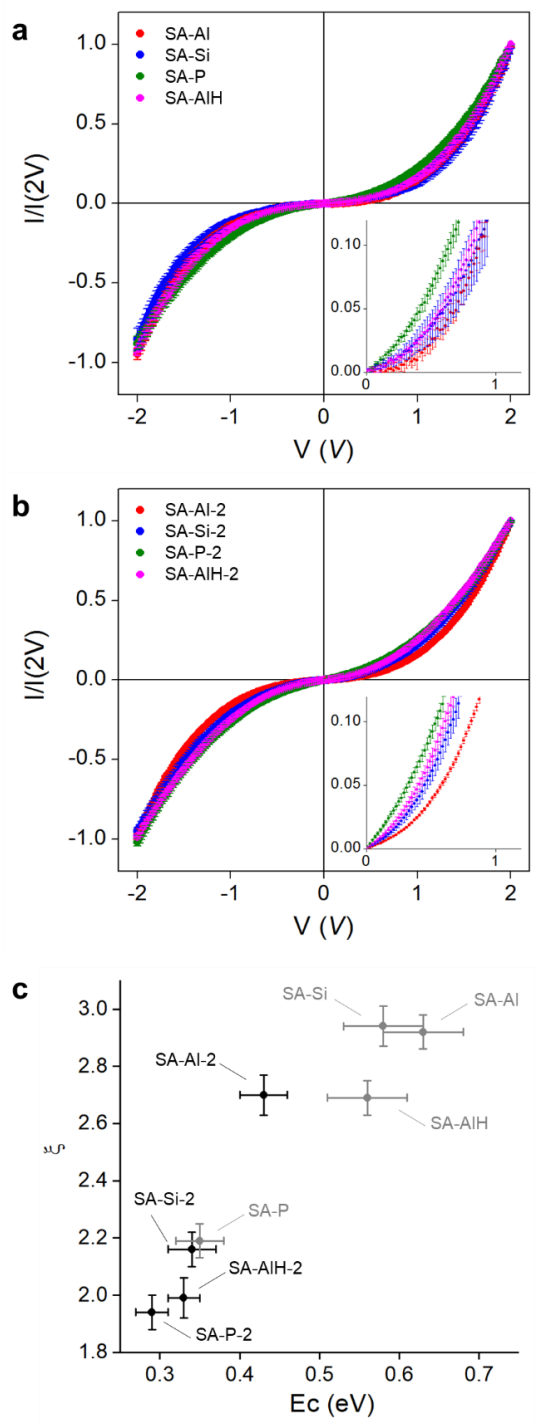

Figure 4. Charge transport measurement at the nanoscale, performed by conductive AFM on the a) **SA-Al**, **SA-Si**, **SA-P**, **SA-AlH** (small nanoparticles) and b) **SA-Al-2**, **SA-Si-2**, **SA-P-2**, **SA-AlH-2** (large nanoparticles) self-assemblies, at room temperature; the curves are normalized at 2 V; insets: magnification on the 0-1 V regions. c) Evolution of the power exponent ξ (fitted from the *I-V* characteristics with small nanoparticles – in grey – and with large nanoparticles – in black) as a function of the corresponding charging energies.